Ultraviolet radiometry with synchrotron radiation and cryogenic radiometry

Ping-Shine Shaw, Keith R. Lykke, Rajeev Gupta, Thomas R. O'Brian, Uwe Arp, Hunter H. White, Thomas B. Lucatorto, Joseph L. Dehmer, and Albert C. Parr

The combination of a cryogenic radiometer and synchrotron radiation enables detector scale realization in spectral regions that are otherwise difficult to access. Cryogenic radiometry is the most accurate primary detector-based standard available to date, and synchrotron radiation gives a unique broadband and continuous spectrum that extends from x ray to far IR. We describe a new cryogenic radiometer-based UV radiometry facility at the Synchrotron Ultraviolet Radiation Facility II at the National Institute of Standards and Technology. The facility is designed to perform a variety of detector and optical materials characterizations. The facility combines a high-throughput, normal incidence monochromator with an absolute cryogenic radiometer optimized for UV measurements to provide absolute radiometric measurements in the spectral range from 125 nm to approximately 320 nm. We discuss results on photodetector characterizations, including absolute spectroradiometric calibration, spatial responsivity mapping, spectroreflectance, and internal quantum efficiency. In addition, such characterizations are used to study UV radiation damage in photodetectors that can shed light on the mechanism of the damage process. Examples are also given for UV optical materials characterization.

OCIS codes: 040.7190, 120.3940, 120.5630.

1. Introduction

Cryogenic radiometers were first developed at the National Institute of Standards and Technology (NIST) and later by the National Physics Laboratory more than 20 years ago.[1–4] A cryogenic radiometer measures the incident radiant power with extremely high accuracy by use of electrical substitution at liquid-helium temperature.[5] To date, cryogenic radiometry is the most accurate primary detector-based standard. Several metrology laboratories are using cryogenic radiometers to realize a scale of absolute spectral response primarily from the near-UV to the near-IR spectral ranges with a remarkable improvement in accuracy. For example, the high-accuracy cryogenic radiometry facility (HACR)[6,7] at NIST uses highly stabilized laser beams for detector calibration in the visible and near-IR spectral ranges. The achieved relative standard uncertainty is less than 0.021%, and the relative standard uncertainty for trap-detector calibration is typically 0.03% at nine laser wavelengths between 406 and 920 nm.[6,7] For short wavelengths the NIST Spectral Comparator Facility (SCF) extends the wavelength to ~200 nm by scale transfer from working standards in a monochromator-based system.[8,9] The scale of the working standard was transferred from HACR-calibrated trap detectors and pyroelectric detectors. The standard uncertainty for UV SCF near 200 nm can be as great as 6.55% (Ref. 9).

For UV, vacuum UV (VUV), and soft-x-ray regions, few choices of light source are available. Conventional laboratory light sources (gas discharge, arc lamp, and plasma sources) have restricted useful spectral ranges and are usually plagued by line structure that results from transitions between discrete energy levels. Unlike conventional light sources, synchrotron radiation (SR) has a unique broadband and smooth spectrum from x ray to far IR with high brightness and low beam divergence.[10] In addition, the properties of the SR beam (such as spectral distribution, polarization, and angular divergence) can be calculated accurately from the machine parameters.[11–14] Two electron-storage rings, namely, the Synchrotron Ultraviolet Radiation Facility (SURF) of NIST[12] and the Berlin electron-storage ring of the Physikalisch-Technische Bundesanstalt (PTB)[15,16] were used to build dedicated detector calibration beamlines for UV, VUV, and x-ray radiation as early as the 1970's. In early experiments a gas

The authors are with the National Institute of Standards and Technology, Gaithersburg, Maryland 20899. The e-mail address for P.-S. Shaw is shaw@enh.nist.gov.

Received 27 May 1998; revised manuscript received 8 September 1998.

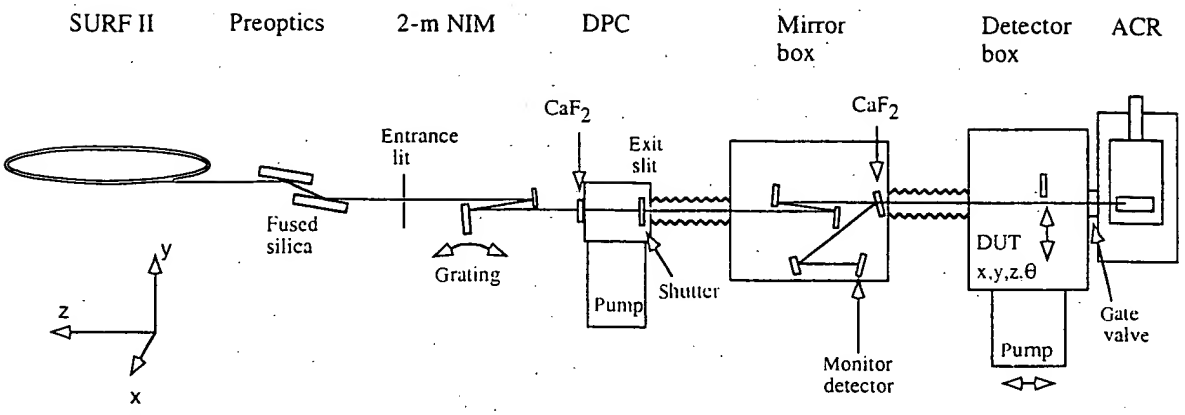

Fig. 1. Schematic diagram of the ACR-based beamline for UV radiometry. NIM, normal incidence monochromator; DPC, differential pumping chamber.

ionization chamber was used as the primary detector standard[17,18] or the storage ring was used as an absolute source standard.[12,19] Only recently, researchers at PTB at the Berlin electron-storage ring first combined a cryogenic radiometer as a primary detector standard with a SR beam for detector calibration in the UV, VUV, and soft x-ray spectral ranges.[16,20,21] They reported a relative standard uncertainty below 1% for most of the spectral range.

At NIST, in response to increasing demand from the industry for improved radiometric accuracy in the UV and VUV regions of the spectrum, a program was initiated to establish a new multipurpose UV radiometric beamline facility at SURF. The new facility is based on an absolute cryogenic radiometer (ACR) as an absolute primary standard to improve standard uncertainties for the spectral range from 125 to 320 nm.[22] This range was selected to complement NIST's UV SCF, where detectors are calibrated with an argon mini-arc lamp and a monochromator for $\lambda >$ 200 nm. The new radiometric beamline extends beyond the spectral range of the UV SCF and includes wavelengths such as 193 and 157 nm, which correspond to excimer laser lines that are particularly of interest for semiconductor photolithography.

Our program has two functions: UV detector characterization and UV optical material characterization. The main goals of UV detector characterization are to measure the absolute spectral responsivity, the uniformity of responsivity, and the stability of the photodetector. In addition, measurement of the spectral reflectance of the test detector can be used to calculate the internal quantum efficiency that is used for the self-calibration of transfer photodiodes.[23,24] In the new radiometric beamline the ACR is used to transfer absolute scales to test detectors. Adjustable slits of the monochromator can adjust the beam size to fit the active area of the test detector. Automated in-vacuum translation stages can map out the spatial uniformity. A UV lens can be placed in the SR beam to focus the beam onto the test detector, and the change of spectral responsivity can be studied as a function of the dosage. An additional monitor diode can be positioned in the vacuum chamber to monitor the reflected beam from the test detector, thus measuring the spectral reflectance from the test detector. Furthermore, the reflectance and the internal quantum efficiency can be monitored during the stability study of the test photodiodes. Such information can shed light on radiation damage mechanisms and help the fabrication of stable UV standard transfer detectors. For characterization of optical material properties, this facility can be adapted easily for other spectroradiometric measurements, including transmittance, reflectance, and scatter.

In this paper we discuss the overall layout of the facility and some recent characterizations (absolute responsivity and reflectance) of new UV detectors. We also discuss the results of UV radiation damage study and its effect on responsivity and reflectance for a number of different UV detectors. We give examples of the research of UV optical materials characterization by measuring the transmittance of fused silica and calcium fluoride windows. Finally, we discuss the upgrade of SURF II to SURF III and possible improvements of the current UV radiometry beamline for the new SURF III storage ring.

2. Beamline Description

The new radiometry facility was constructed on beamline 4 at SURF II. The schematic of the beamline components is shown in Fig. 1. The SR beam from SURF II is collected and imaged onto the entrance slit of a 2-m monochromator by a preoptics system.[25,26] Monochromatic light from the monochromator is reimaged again by two mirrors in the mirror box. Downstream of the mirror box is a vacuum detector box in which the device under test (DUT) is installed. The design of the box is such that there is enough room and flexibility for a variety of measurements. Connected to the back side of the detector box is the ACR for accurate power measurement.

To measure the power of the SR beam that irradiates the test device, one must ensure that the cavity of the ACR is close to the focal position of the monochromatized SR beam and that the beam underfills

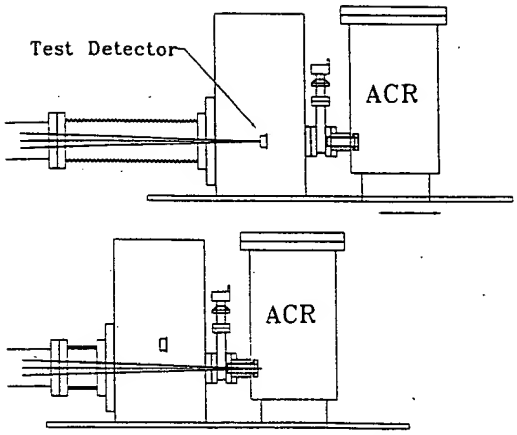

Fig. 2. Positioning of the test detector and the ACR to bring the test detector or the ACR to the focal position of the SR beam. The ACR measures the total power of radiation when the ACR is in the focal position, and the response of the test detector is measured when the test detector is positioned in the focal position.

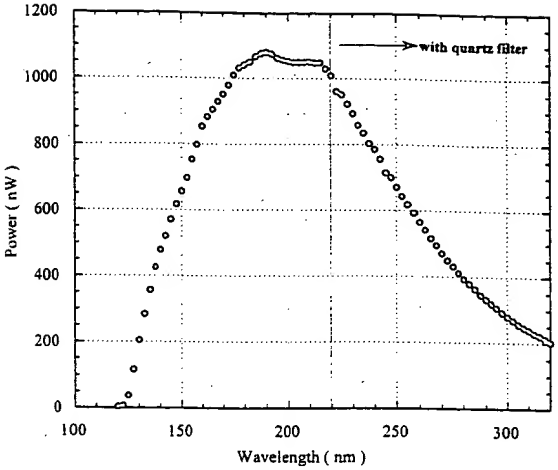

Fig. 3. Measured optical power output from the beamline monochromator with 90 mA of electron-beam current and a slit size of 3×3 mm^2 (~2-nm resolution). In this measurement a quartz window was inserted before the exit slit to suppress higher-order light when the wavelength setting of the monochromator was longer than 220 nm.

the cavity. This condition prevents loss of light that is due to the divergence of the SR beam. Ideally, one should then be able to position the detector to be calibrated at the position of the ACR when the total power was measured. Also, all movements must be done under vacuum for proper operation of the ACR. One approach for achieving this condition by the PTB[21] and the National Research Council of Canada[27] is to position both the ACR and the test detector in a plane perpendicular to the beam (synchrotron for the PTB, lamp or monochromator for the NRC). In these setups one or two vacuum bellows were used to connect the ACR and the test detector to the beamline that provides flexibility in the motion of the ACR and the test detector. A linear motion, in the direction perpendicular to the SR beam, brings the ACR or the test detector into the focal position. Another more recent approach by the PTB encloses the entire ACR and the test detector into one vacuum chamber. Motions inside the chamber can move either the ACR or the test detector to the focal position. This approach is intended mainly to reduce the positioning uncertainty that is due to large excursion of the vacuum enclosure to position the ACR and the test detector into the optical path.

To simplify the motion under vacuum and to reduce the size of the facility, our approach places the detector box and the ACR in line with the SR beam, and both are positioned on a single translation stage that moves parallel to the SR beam. In this way either the ACR or the test detector can be placed at the focal position with a moving distance of ~18 cm in this facility. A second motion perpendicular to the beam allows one to move the test detector inside the detector box in and out of the beam. The movements are illustrated in Fig. 2. It is important that the SR beam underfill the ACR cavity to avoid systematic error. One can adjust the alignment either by moving the ACR manually or by adjusting the focusing optics in the mirror box. So that proper alignment was ensured, the signal from ACR was monitored while the ACR was moved in the direction of the SR beam. When properly aligned, the ACR could be moved more than 2 cm before a 0.1% change was observed.

A. Preoptics and Monochromator System

The preoptics and monochromator systems have been described in detail elsewhere.[25,26] In short, two grazing incidence (80°) fused-silica mirrors, one plane and the other toroidal, make a 1:1 image of the SR beam from the storage ring on the entrance slit of the 2-m monochromator. The monochromator has a normal incidence mirror and a curved grating with 600 lines/mm and blazed at 200 nm. The exit slit of the monochromator is made up of two sets of adjustable slits to control the resolution and the size of the exit beam in both horizontal and vertical directions. With these slits the SR beam size can be adjusted according to the area of the test detector. The resolution is 0.7 nm at 200 nm when the horizontal slit is 1 mm wide (the grating disperses in the vertical direction). The preoptics and monochromator system accepts 65 mrad horizontally and 12 mrad vertically of the SR beam. The system generally delivers approximately a microwatt of radiant power near 200 nm. An example of a typical monochromator output power spectrum is shown in Fig. 3 with the SURF electron beam operated at an energy of 256 MeV and a current of 90 mA. Note that, for wavelengths longer than 220 nm, a fused-silica filter was inserted into the beam to suppress higher-diffraction-order contributions. For comparison, we calculated the spectral radiance of SURF II from Schwinger's equation.[13] With 90 mA of electron-beam current, the beamline optics collect 157 μW nm^{-1} of the SR beam at a wavelength of 200 nm. This calculation shows that the throughput of the optical system is

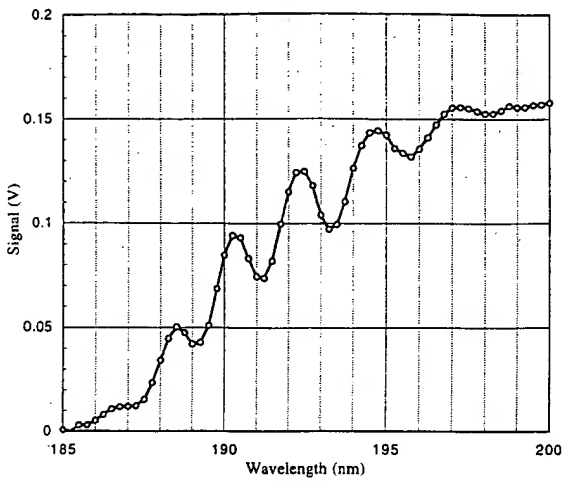

Fig. 4. Measured spectral response of a photodiode in the air-filled detector box from 180 to 200 nm. The oxygen Schumann–Runge bands are used for wavelength calibration.

lower than expected. We are currently investigating the optical system to improve the throughput for the new SURF III project.

For wavelength calibration, the SR beam is transmitted through air before it impinges on a photodiode. The measured Schumann–Runge bands of oxygen between 180 and 200 nm are then compared with those measured with a separate calibrated monochromator system with similar resolution. Wavelength uncertainty of the 2-m monochromator in this UV region is 0.1 nm. The measured Schumann–Runge bands are shown in Fig. 4.

The spectral purity of the monochromator is determined by two methods: (1) by use of a separate monochromator to scan the output beam of the 2-m monochromator and (2) by measurement of the total scattered light emanating from the exit slit below the spectral cutoff with a fused-silica filter and a photodiode when the monochromator is tuned slightly above the cutoff of the fused-silica filter. Our results show that the total out-of-band stray light contribution is below 1×10^{-3} of the radiant power output from the monochromator.

The spatial characteristics of the beam were observed with a CCD camera to study the beam size, beam divergence, and astigmatism. These quantities affect the design of the optical system, which has to be properly adapted to ensure complete light collection by the ACR and test detector. Angular spread of the incident light on the test detector can affect the detector responsivity.[27] The measured beam divergence is approximately 1° in the vertical direction and 2° in the horizontal direction, in accordance with the geometry of the collection optics of the monochromator.

Finally, an in-vacuum shutter was installed immediately before the exit slits of the monochromator. This shutter is mainly used for measurement of the background bias power of the ACR. We studied the thermal radiation from the shutter before and after every ACR scan by closing another shutter (gate valve) at the beginning of the beamline. The gate valve shutter was in turn checked for thermal background when there was no electron beam in the storage ring. The thermal effect of the shutter was determined to be less than 10 nW. This background was subtracted from all of the ACR measurements.

B. Mirror Box

Connected to the exit slit of the 2-m monochromator is a vacuum mirror box that contains the refocusing optics that image the SR beam from the monochromator exit slit onto the test detector or the ACR with 1:1 magnification. There are two Al–MgF_2 mirrors, one plane and one spherical, aligned at near-normal incidence to the SR beam.

A CaF_2 window is inserted into the light path as a beam splitter to reflect a small portion of the beam onto a monitor photodiode. The signal from the monitor diode is used to normalize the signal either from the test detector or from the ACR. The monitor signal is important, since it allows the detector signal to be normalized to the gradual decay of the electron beam in the storage ring and to any fluctuations caused by motions of the optics upstream of the mirror box.

The vacuum of the mirror box and of the detector box is separated from the vacuum of the monochromator by a CaF_2 window. This reduces the sample turnaround time to a few minutes, because ultrahigh vacuum is not required for operation in the mirror box and in the detector box. However, ultrahigh vacuum is required for the monochromator vacuum, which is open to the SURF electron-storage ring. The CaF_2 window limits the spectral range to $\lambda > 120$ nm. For future calibrations below 120 nm, this window will be removed.

C. Detector Box

A flexible vacuum bellows connects the detector box to the mirror box so that, as mentioned below, the test detector in the detector box and in the cavity of the ACR can be moved into and out of the focal position. Inside the box, in-vacuum stages hold a platform where the DUT can be mounted. There are a total of three motion stages, two linear translation stages to position the DUT in the x–y plane (the plane perpendicular to the SR beam), and one rotation stage to adjust the incidence angle of the SR beam on the DUT. The linear stages for x–y motions can raster the DUT for spatial uniformity measurements and the profile measurements of the SR beam. The x–y motion also moves the DUT in and out of the optical path to make alternate measurements between the DUT and the ACR.

The detector box is designed with maximum flexibility for a variety of measurements. Several devices can be mounted simultaneously to the DUT platform. For example, a photodiode with a small aperture can be mounted alongside the detector to study the SR beam profile, and additional monitor diodes can also be mounted to measure the reflec-

tance and transmittance of the DUT. A thermocouple temperature probe is also provided in the detector box to monitor the temperature of the DUT. The inner walls of the detector box are coated with a thin layer of black graphite to suppress the scattered light in the box. In particular, care must be taken to properly suppress backreflected light from the DUT. In the case of photodiodes, the detector is slightly tilted to ~2° from normal incidence so that most of the backreflected light is absorbed by the walls of the detector box.

As mentioned above, the detector box and the ACR are connected together in line by means of a vacuum gate valve. The detector box and the ACR assembly are mounted on an external linear translation stage for motion in the z direction (the direction of the SR beam). The z-motion linear stage, along with the in-vacuum stages in the detector box, are controlled with a single computer. An automation software program coordinates all the motions to bring the ACR and the DUT to the focal position of the SR beam sequentially.

D. Absolute Cryogenic Radiometer

The principles and performance of the ACR have been discussed extensively in the literature.[3–7] For this study the ACR from Cambridge Research and Instrumentation[28] is equipped with two-stage, liquid-nitrogen and liquid-helium, cooling for the receiver cavity. The electroformed copper cavity is operated at a nominal temperature of 4.2 K to decrease the heat capacity and increase the thermal conductivity to allow for a quick time response. The entrance opening of the cavity is 8 mm in diameter, and the interior surface is coated with chromium oxide for maximum UV absorption. The temperature of the receiver cavity is actively stabilized with electrical power to a temperature just above 4.2 K, and the cavity has a thermal link to an actively stabilized heat sink connected to a liquid-helium-cooled dewar. The cavity has a thermal responsivity of 3.2 mK μW^{-1} with a time constant of a few seconds.

Since both the ACR and the DUT operate under vacuum conditions, the entrance window for the ACR is no longer needed. This eliminates the need for precision measurement of the window transmittance and the uncertainty associated with this measurement for an in-air ACR system such as the NIST HACR facility.[6,7]

The performance of the ACR was characterized with a He–Ne laser before the ACR was installed on the SURF beamline for cavity absorptance and nonequivalence study. The cavity absorptance was measured to be better than 0.9994. With 0.1–2 mW of laser power, the relative standard uncertainty components from the power measurement scale factor, the cavity absorptance, and nonequivalence were found to be 0.013%, 0.0002%, and 0.0006%, respectively. The combined relative standard uncertainty is 0.014%.

After the ACR was installed on the beamline, another intercomparison was performed with the NIST

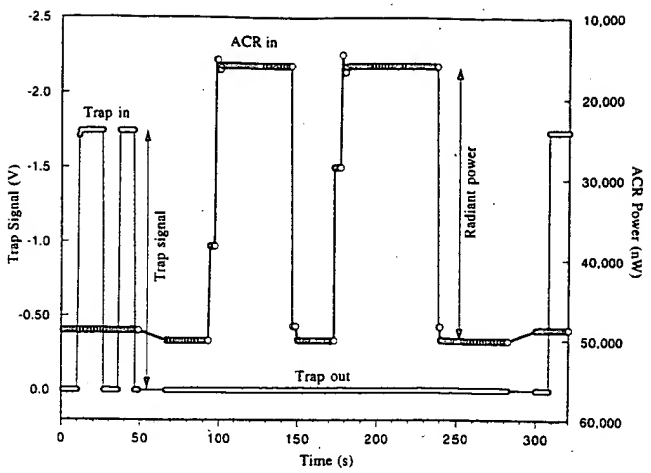

Fig. 5. Time scan of the trap-detector response and the ACR power measurement with a He–Ne laser. The trap detector is a transfer standard that was precalibrated by HACR. The apparent background change for the ACR power measurement results from use of the ACR for viewing either the back of the trap detector (for measuring the trap detector response) or the proper background that views the beamline.

HACR by use of a trap transfer detector with an intensity stabilized He–Ne laser at 632.8 nm. The trap detector was placed in the detector chamber under vacuum. The laser was directed into the detector through a vacuum window and alternately irradiated the trap detector then the ACR. The power of the laser was attenuated to a range from approximately 30 to 4 μW to approach the actual power from the SR beam instead of the typical milliwatt power used for laser radiometry. The laser beam size was ~1 mm, and the divergence was less than 1 mrad. No effect was observed for the trap-detector response in air or in vacuum at this laser wavelength. Shown in Fig. 5 is a time scan of the signal from the trap detector and the beamline ACR. Two successive measurements from the ACR of the incident light were used to correct for the drift of the ACR baseline value that is due to slow variation of thermal background. Typical drift is relatively linear and less than 10 nW over the time scale of the measurement. The responsivity of the trap detector obtained from the beamline ACR measurements agreed within 0.1% of the value obtained from the HACR measurements.

The dominant contribution of the uncertainty of the beamline ACR measurement arises from the statistics of the power measurement. We found a typical rms noise value of 2 nW from the ACR's power measurement. For an incident SR beam power of 1 μW, the relative standard uncertainty of the power measurement was therefore as great as 0.2%.

For measurement in the UV and VUV ranges, another factor that has to be considered is the cavity absorptance. The absorptance of the cavity is generally assumed to be 0.999 in the UV and VUV ranges.[21] This is reasonable from the measured cavity absorptance value of 0.9994 at 632.8 nm and the

relative flat spectral response of cavity absorptance. In the worst case, the relative standard uncertainty of absorptance is estimated to be its actual value of 0.1%. Thus the total combined relative standard uncertainty of the ACR is 0.22% for 1-μW incident power in the UV and VUV ranges.

3. Detector Characterization

The most important radiometric characterization of a solid-state detector is the measurement of the absolute spectral responsivity. The responsivity is expressed as current per unit incident power (in amperes per inverse watts) for a typical solid-state detector. Furthermore, when the reflectance of the detector is measured, the internal quantum efficiency can be deduced from both the absolute responsivity and the reflectance. The internal quantum efficiency, as defined by the number of electrons generated in the detector per absorbed photon, is a fundamental quantity of the solid-state detector that can be modeled by basic electronic properties of the detector materials. For silicon-based photodiodes, the internal quantum efficiency is close to unity in the visible range. Because of this self-calibrating property of the photodiodes, silicon-based photodiodes have become the most important transfer detectors for detector-based radiometry.[23,24]

An important criterion for a candidate of the transfer standard detector is the uniformity of the responsivity across the sensitive area of the detector. Poor uniformity makes the measured responsivity dependent on the shape of the probe beam and increases the measurement uncertainty.

We studied several different types of UV detector, using the new radiometric beamline. These include silicon *p*-on-*n* (Hamamatsu Models 1337 and 5227), silicon *n*-on-*p* (International Radiation Detectors Model UVG and UDT Model UV100), Schottky-type PtSi-*n*-Si (Institute for Quantum Electronics, Swiss Federal Institute of Technology), GaN (APA Optics), GaP (Hamamatsu), GaAsP (Hamamatsu), and diamond photoconductive (Alameda Applied Sciences).[28] The measurements and some of the results are discussed below.

A. Absolute Spectral Responsivity and Uniformity

The measurement of absolute spectral responsivity involves alternating exposure of the DUT and the ACR to the SR beam. The ACR measures the absolute power of the radiation, and the monitor diode monitors the relative power change of the SR beam between the measurements of the ACR and the DUT.

The actual procedure for spectral responsivity measurement is demonstrated in Fig. 6. At each wavelength the measurement sequence is as follows: (1) The ACR is moved to the focal position, and the shutter is closed to measure the background bias power of the ACR; once the data from the ACR is recorded, the shutter is opened and the electrical power of the ACR is measured with the SR beam irradiating the cavity. (2) The DUT is moved to the focal position and positioned such that the SR beam irradiates the sensitive

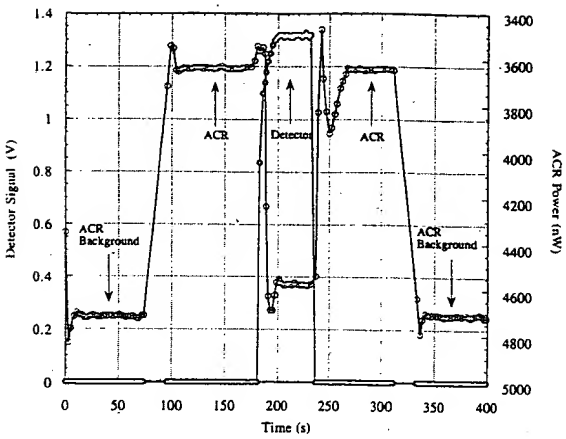

Fig. 6. Data collection process for measuring the spectral responsivity of the detector. The measurement cycle for each wavelength is as follows: (1) Move the ACR to the focal position, close the shutter, and measure the ACR background. (2) Open the shutter, and measure the ACR power. (3) Move the detector to the focal position, and measure the signal of test detector from the current-to-voltage amplifier. (4) Move the ACR to the focal position, and measure ACR power. (5) With the shutter closed, measure the ACR background.

area of the DUT at a predefined position; one measures the current response of the DUT by reading the voltage signal from a current-to-voltage amplifier. (The detector background is obtained while the ACR reading is taken in step 1.) (3) The ACR is moved back to the focal position, and the ACR power is measured again both with the shutter open and with the shutter closed, as in step 1. Steps 1 and 3 give the ACR power drift caused by slow variation of thermal background. Note that the monitor diode monitors the SR beam throughout the entire measurement sequence. All the data from the DUT and the ACR are normalized with the monitor signal to account for the decay of the SR beam.

Shown in Fig. 7 are the spectral responsivities for a representative sampling of photodetectors between 120 and 320 nm. The diamond photoconductive detector was operated with a bias voltage of 90 V, and the absolute spectral responsivity shows an interesting long-wavelength cutoff near 230 nm. This long-wavelength cutoff is a result of the large bandgap and high transmittance of diamond in the longer wavelength. However, it is not clear at the present time why there is a nonnegligible responsivity above the cutoff wavelength. Owing to the small size (1 mm × 3 mm) of the active area of the diamond photoconductive detector, the spatial uniformity cannot be measured with this facility. Also noticeable in Fig. 7 is the structure exhibited by the silicon *n*-on-*p* photodiode caused by the etalon effect from the surface layer of the photodiode.

The spatial uniformity of the detector responsivity directly influences the measurement uncertainty of a detector. One can measure the spatial uniformity of a DUT by scanning the DUT in the plane that is normal to the SR beam by x and y

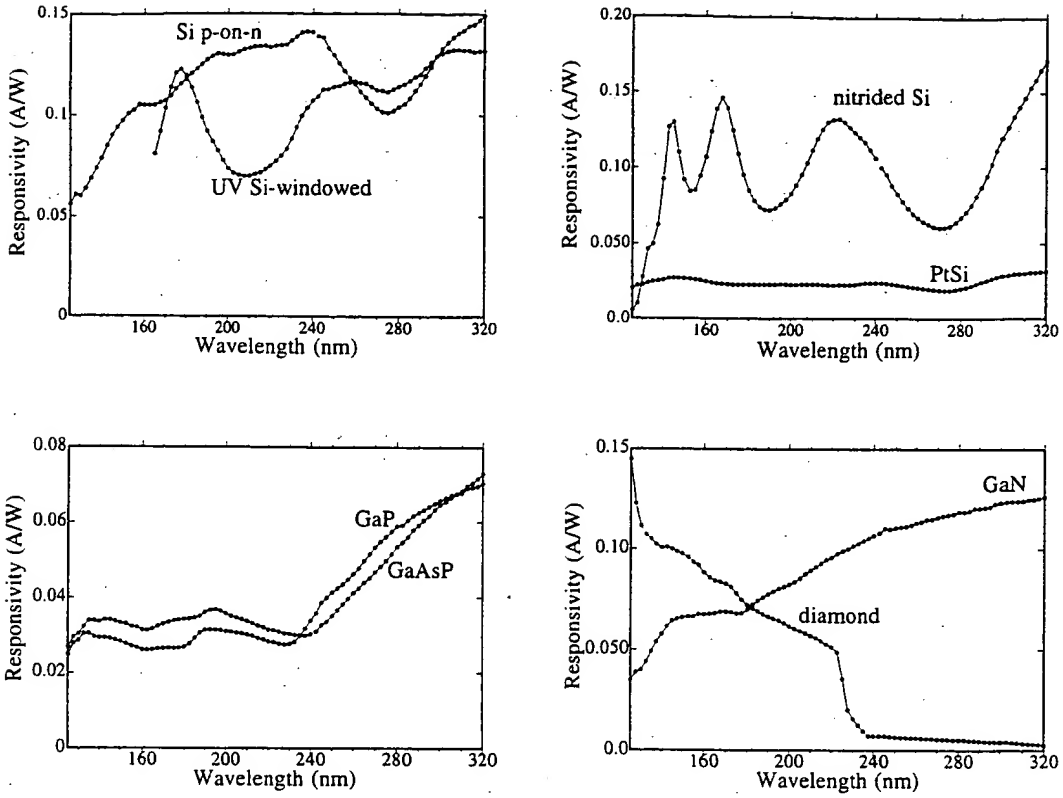

Fig. 7. Measured spectral responsivity for UV photodetectors of silicon p-on-n (Hamamatsu 1337), nitrided silicon n-on-p (IRD UVG), silicon n-on-p with protective window (UDT UV100), Schottky-type PtSi-n-Si, GaN, GaP, GaAsP, and diamond photoconductive detector. A bias voltage of 90 V was used for diamond photoconductive detector measurement.

stages. The typical beam size is set to 1 mm by adjustment of the monochromator exit slits. Shown in Fig. 8 is a uniformity scan of a GaN diode at 180 nm.

Our analysis of the error budget for the absolute responsivity measurement showed that there are two major sources of type A uncertainties (i.e., uncertainties of statistical origin[29]). One is from the noise floor of the ACR (~2 nW). At 200 nm the output power is typically 1 μW and the relative standard uncertainty is 0.20%. At wavelengths of 300 and 135 nm, the relative standard uncertainties increase to 0.60%. Another source of error resulted from the fast oscillation of the SR beam. This oscillation (~100 Hz) causes fluctuation in the photodiode signal. Electronic filtering (low pass at 3 Hz) of the photodiode signal reduces noise to a relative standard uncertainty of 0.30%. This oscillation has no effect on the ACR, owing to the long time constant of a few

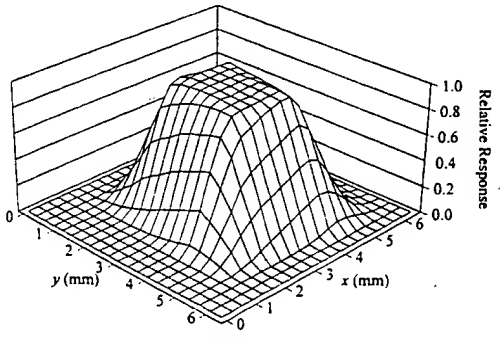

Fig. 8. Measured spatial uniformity of a GaN photodiode at 180 nm.

Table 1. Components of the Combined Relative Standard Uncertainty of Spectral Responsivity[a]

Source of Uncertainty	Component of Uncertainty (%)
ACR power measurement	
With 1-μW optical power	0.22
With 0.3-μW optical power	0.62
Monitor diode current measurement	0.30
Test diode current measurement	0.30
Wavelength scale and spectral bandwidth[b]	0.25
Out-of-band stray light	0.10
Test diode positioning[b]	0.20
Combined	
With 1-μW optical power	0.56
With 0.3-μW optical power	0.81

[a]The 1-μW optical power of the monochromatic SR beam is the typical power at 200 nm, and the 0.3-μW optical power is the typical power at 175 and 300 nm.

[b]These uncertainties are dependent on the spectral responsivity and spatial uniformity of the test diode. The numbers in this table are for relatively slowly varying spectral responsivity and good spatial unformity, as are most of the photodiodes reported in this study.

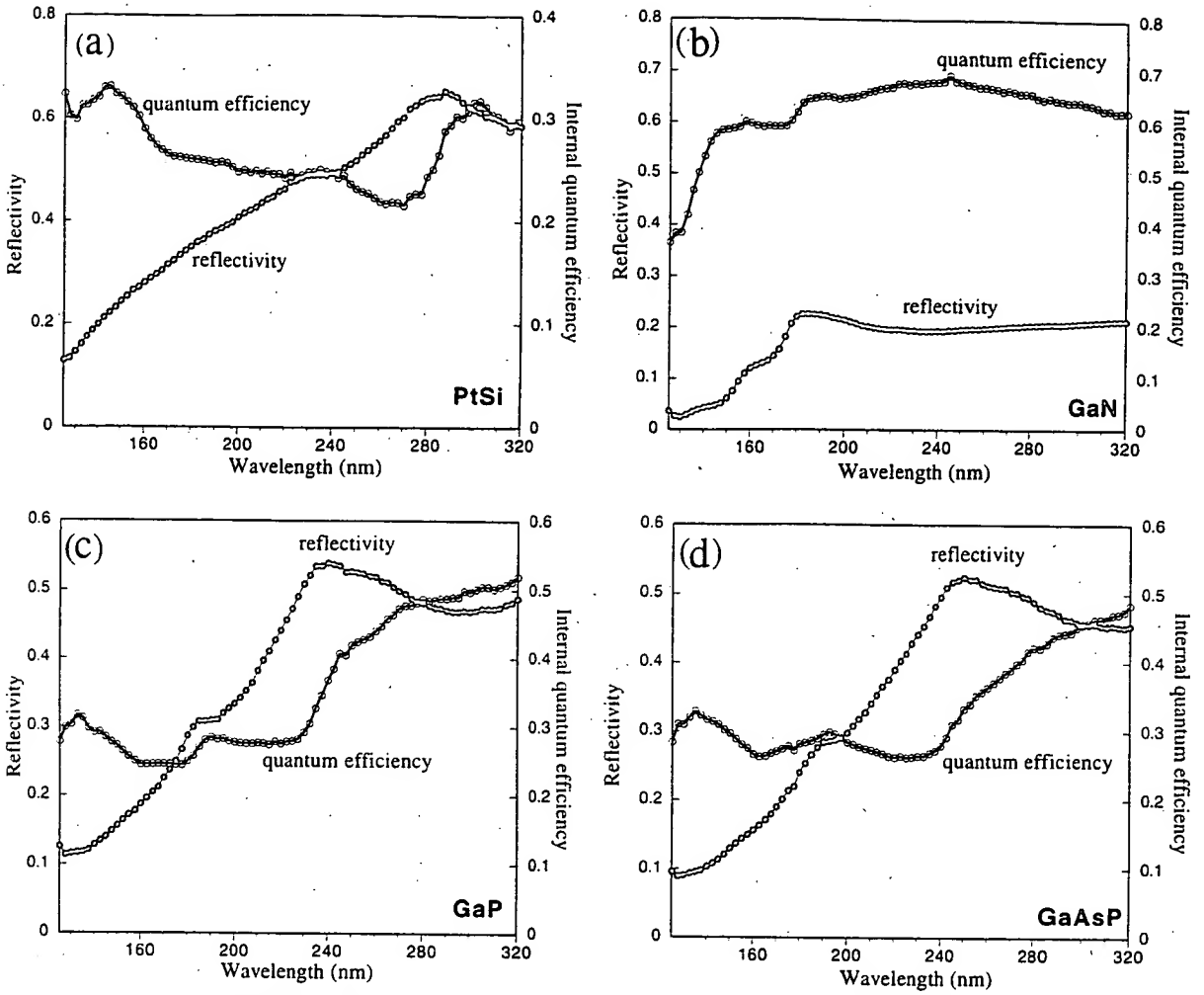

Fig. 9. Reflectance and internal quantum efficiency for PtSi, GaN, GaP, and GaAsP photodiodes.

seconds. The uncertainty components of the spectral responsivity are listed in Table 1. At 200 nm the combined relative standard uncertainty is 0.56%. At wavelengths of 300 and 135 nm the combined relative standard uncertainties increase to 0.81%, because of the lower power of the SR beam from the monochromator and the larger uncertainty from the ACR power measurement.

B. Reflectance and Internal Quantum Efficiency

For the reflectance of a photodiode to be measured, the SR beam is arranged to impinge on the photodiode at a near-normal incidence angle. A second reference photodiode is placed in the detector box to collect the reflected light from the test photodiode. Both diodes' responsivities are calibrated before the reflectance measurement.

The reflectance of the diodes can be obtained by measurement of the power of the SR beam impinging on the photodiode (the current of the photodiode divided by the responsivity of the diode) and the power of the reflected light. The signal from the photodiode divided by the signal from the reference diode is given by the following equation:

$$\frac{V_p(\lambda)}{V_r(\lambda)} = \frac{P(\lambda)S_p(\lambda)}{r(\lambda)P(\lambda)S_r(\lambda)}, \tag{1}$$

where $V_p(\lambda)$ and $V_r(\lambda)$ are the measured signal, which can be voltage or current from the test photodiode and the reference photodiode, respectively. $S_p(\lambda)$ and $S_r(\lambda)$ are the responsivity of the test photodiode and the reference photodiode, respectively. $r(\lambda)$ is the reflectance of the test photodiode, and $P(\lambda)$ is the incident power.

The reflectance can then be calculated by

$$r(\lambda) = \frac{V_r(\lambda)S_p(\lambda)}{V_p(\lambda)S_r(\lambda)}. \tag{2}$$

The relation among the internal quantum efficiency $q_{\text{int}}(\lambda)$ in electrons per photon, the responsivity $S_p(\lambda)$ in ampheres per watt, and the reflectance of the test photodiode is[30]

$$S_p(\lambda) = [1 - r(\lambda) - a(\lambda)]\frac{e}{h\nu}q_{\text{int}}(\lambda), \tag{3}$$

where e is the charge of an electron, $h\nu$ is the photon energy, and $a(\lambda)$ is the absorption of the surface layer of the photodiode.

For photodiodes with no or negligible surface layer absorption $a(\lambda)$, we have

$$q_{\text{int}}(\lambda) = \frac{h\nu}{e} \frac{S_p(\lambda)}{1 - r(\lambda)}. \quad (4)$$

Shown in Fig. 9 are the measured reflectance and internal quantum efficiency for four different photodiodes, PtSi, GaN, GaP, and GaAsP. Unlike silicon p-on-n and n-on-p photodiodes, all four photodiodes have quantum efficiencies of less than 1 for the wavelength region of 125–320 nm. They also have lower reflectance than silicon p-on-n and n-on-p photodiodes in this wavelength region.

C. Detector Ultraviolet Radiation Damage

As mentioned above, one of the main goals of this new radiometric beamline is to characterize existing UV detectors and to find candidates that are suitable as UV transfer standards. However, it is well known that most UV photodiodes are subject to UV radiation damage.[31–33] UV radiation damage of the photodiode can cause great calibration uncertainties.

For studying the effects of UV radiation damage, the exit slit of the monochromator was completely opened and a CaF_2 lens was inserted into the optical path to further focus the beam to approximately 1 mm × 1 mm onto the DUT. This increases the power density of the UV radiation on the detector to ~0.08 mW cm^{-2} at 135 nm. For the research reported here, UV dosage on the detector was with 135-nm light. The choice of 135 nm is a balance between the high photon energy and available power from the beamline.

Shown in Fig. 10 is the change in responsivity of silicon p-on-n, nitrided silicon n-on-p, and Schottky-type PtSi-n-Si photodiodes as a function of the UV dosage. The nitrided silicon n-on-p and Schottky PtSi-n-Si are much more UV resistant, thus making these photodiodes good candidates for UV transfer standards and devices such as trap detectors.[34] The changes in absolute spectral responsivity and reflectance for the Hamamatsu 1337 silicon p-on-n diode from the UV radiation damage are shown in Fig. 11. It can be seen from this figure that there is a significant drop in the absolute spectral responsivity before and after radiation damage in the range of our measurement. However, there is no dramatic change in the shapes of both the absolute spectral responsivity and the reflectance. Possible damage mechanisms include the creation of semiconductor trap states by UV radiation. These trap states induce electron–hole pair recombination loss that is independent of the photon energy.[30,31] We plan to conduct more studies on the mechanism associated with the radiation damage.

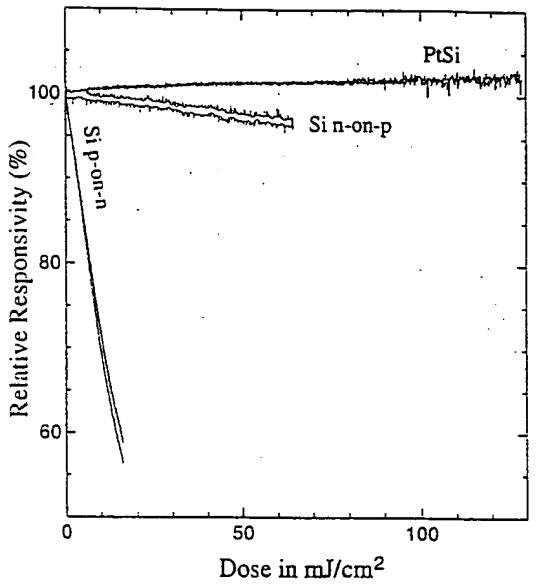

Fig. 10. Change of detector responsivity from 135-nm UV radiation for (a) Hamamatsu 1337, (b) Hamamatsu 5227, (c) International Radiation Detectors silicon, (d) PtSi photodiodes.

4. Optical Material Characterization

The new radiometric beamline can be adapted easily to measure UV transmittance, reflectance, and scattering. To demonstrate this capability, we measured the UV transmittance of fused silica and CaF_2. The test sample was held on the in-vacuum stages in the detector box. A fixed photodiode was positioned in the optical path in the detector box. We measured the absolute transmittance and spatial variation of the transmittance by moving the sample in and out of the beam. The result is shown in Fig. 12 for the transmittance of fused silica and CaF_2.

The high-precision measurement of optical properties requires careful treatment of sample surfaces and suppression of the scattered or backreflected light to keep it from being detected by the photodiode. Other effects involve angular alignment and polarization effects from the birefringent properties of the sample. It is a challenge to account for all these effects when precision measurements of optical quan-

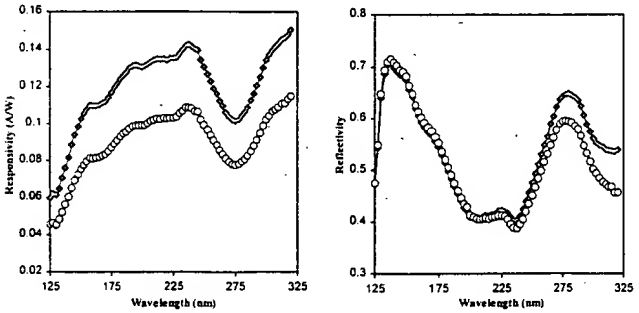

Fig. 11. Measured change of absolute spectral responsivity and reflectance of a Hamamatsu Si 1337 photodiode. Diamonds are before and circles are after 135-nm UV radiation for a total dose of 16 mJ cm^{-2}.

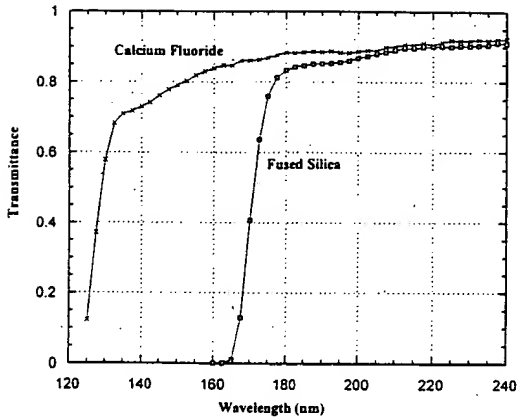

Fig. 12. UV transmittance of two samples, calcium fluoride and fused silica, measured with the new radiometric beamline.

tities to less than 1% uncertainty are required. However, such accuracy in this wavelength region will become necessary as the semiconductor industry uses ever shorter wavelengths for device fabrication. We are currently evaluating the uncertainties in our measurements and intercomparing our results with independent studies. The result will be discussed in a future publication.

5. Conclusion and Outlook

We have constructed an ACR-based UV radiometry facility at beamline 4 of SURF II. This facility complements the spectral range of NIST's SCF with improved accuracy of the radiometric scale in the UV region. Currently, the spectral range of the facility is extended from approximately 125 to 320 nm with relative standard uncertainty of less than 1%. This facility is capable of characterizing UV detectors by measurement of the absolute spectral responsivity and reflectance of detectors. With these measurements, internal quantum efficiency can be readily obtained. In addition, this facility can be used to study the stability of UV detectors under UV radiation. Changes in responsivity, reflectance, and internal quantum efficiency can be separately monitored during the radiation damage process. A variety of photodetectors have been tested for their UV characteristics as part of our effort to develop UV transfer standards and UV trap detectors. We also give examples of using this facility for optical materials characterization. Properties such as reflectance, transmittance, and scattering can be studied readily with the new facility.

SURF II is currently undergoing a major upgrade to SURF III. The main goal is to establish SURF III as a highly accurate absolute radiometric light source. For this goal to be accomplished, major upgrades in the storage ring magnet will improve the uniformity of the magnetic field and significantly reduce the uncertainty of the magnetic field. This along with a more accurate measurement of the electron-beam current will reduce the relative standard uncertainty of the absolute spectral irradiance of SURF III to less than 0.5% from IR through the vacuum UV (VUV) spectral range.[35] SURF III will have one or more beamlines dedicated to source-based radiometry. For UV radiometry the current configuration of the ACR-based radiometry beamline limits the short-wavelength range to 125 nm because of CaF_2 window transmittance. We plan to upgrade the beamline to a windowless system, and the spectral range can be extended to ~50 nm for the new SURF III machine. For research that requires high-spectral-purity light, such as the characterization of filters, gratings, and filter radiometers, a high-purity monochromator system is also being planned for SURF III. With all these developments, SURF III is expected to have a major impact in the growing field of UV radiometry.

The authors thank Robert Madden, Lanny Hughey, Andrew Hamilton, and Mitchell Furst for their help in the design and operation of beamline 4 and Randall Canfield and Robert Vest for valuable discussions on the calibration and the stability of photodiodes. We also thank Duane Enderle and Steve Runkles for the construction of vacuum chambers. Hunter H. White was a NIST summer undergraduate research fellow supported by NIST and the National Science Foundation when this study was performed.

References and Notes

1. D. C. Ginnings and M. L. Reilly, "Calorimetric measurement of thermodynamic temperatures above 0 °C using total blackbody radiation," in *Temperature: Its Measurement and Control in Science and Industry*, H. H. Plumb, ed. (Instrument Society of America, Pittsburgh, Pa., 1972), Vol. 4, Part I, pp. 339–348.
2. C. R. Yokley, "Long wave infrared testing at NBS," in *Applications of Optical Metrology: Techniques and Measurements II*, R. C. Harney, ed., Proc. SPIE **416**, 2–8 (1983).
3. T. J. Quinn and J. E. Martin, "A radiometric determination of the Stefan–Boltzmann constant," in *Precision Measurement and Fundamental Constants II*, Natl. Bur. Stand. (U.S.) Spec. Publ. **617**, 291–297 (1984).
4. T. J. Quinn and J. E. Martin, "A radiometric determination of the Stefan–Boltzmann constant and thermodynamic temperature between −40 °C and +100 °C," Philos. Trans. R. Soc. London Ser. A **316**, 85–189 (1985).
5. J. E. Martin, N. P. Fox, and P. G. Key, "A cryogenic radiometer for absolute radiometric measurements," Metrologia **21**, 147–155 (1985).
6. T. R. Gentile, J. M. Houston, and C. L. Cromer, "Realization of a scale of absolute spectral response using the National Institute of Standards and Technology high-accuracy cryogenic radiometer," Appl. Opt. **35**, 4392–4403 (1996).
7. T. R. Gentile, J. M. Houston, J. E. Hardis, C. L. Cromer, and A. C. Parr, "National Institute of Standards and Technology high-accuracy cryogenic radiometer," Appl. Opt. **35**, 1056–1068 (1996).
8. T. C. Larason, S. S. Bruce, and C. L. Cromer, "The NIST high accuracy scale for absolute spectral response from 406 nm to 920 nm," J. Res. Natl. Inst. Stand. **101**, 133–140 (1996).
9. T. C. Larason, S. S. Bruce, and A. C. Parr, "NIST measurement services: spectroradiometric detector measurements: Parts I and II—ultraviolet and visible to near infrared detectors," Natl. Inst. Stand. Technol. (U.S.) Spec. Publ. **250–41** (1997).

10. See, for example, G. Margaritondo, *Introduction to Synchrotron Radiation* (Oxford U. Press, New York, 1988), Chaps. 1 and 2.
11. D. L. Ederer, E. B. Saloman, S. C. Ebner, and R. P. Madden, "The use of synchrotron radiation as an absolute source of VUV radiation," J. Res. Natl. Inst. Stand. Technol. **79 A** 761–774 (1975).
12. M. L. Furst, R. M. Graves, L. R. Canfield, and R. E. Vest, "Radiometry at the NIST SURF II storage ring facility," Rev. Sci. Instrum. **66,** 2257–2259 (1995).
13. J. Schwinger, "On the classical radiation of accelerated electrons," Phys. Rev. **75,** 1912–1925 (1949).
14. B. Wende, "Radiometry with synchrotron radiation," Metrologia **32,** 419–423 (1996).
15. G. Ulm, and B. Wende, "The radiometry laboratory of PTB at BESSY," Rev. Sci. Instrum. **66,** 2244–2247 (1995).
16. H. Rabus, F. Scholze, R. Thornagel, and G. Ulm, "Detector calibration at the PTB radiometry laboratory at BESSY," Nucl. Instrum. Methods A **377,** 209–216 (1996).
17. L. R. Canfield, "New far UV detector calibration facility at the National Bureau of Standards," Appl. Opt. **26,** 3831–3837 (1987).
18. L. R. Canfield and N. Swanson, "Far ultraviolet detector standards," J. Res. Natl. Bur. Stand. **92,** 97–112 (1987).
19. R. E. Vest, L. R. Canfield, M. L. Furst, R. P. Madden, and N. Swanson, "Dual grating monochromator for detector calibrations using synchrotron radiation as an absolute source at NIST," Nucl. Instrum. Methods A **347,** 291–294 (1994).
20. A. Lau-Frambs, U. Kroth, H. Rabus, E. Tegeler, G. Ulm, and B. Wende, "First results with the new PTB cryogenic radiometer for the vacuum ultraviolet spectral range," Metrologia **32,** 571–574 (1995/1996).
21. H. Rabus, V. Persch, and G. Ulm, "Synchrotron-radiation-operated cryogenic electric-substitution radiometer as the high-accuracy primary detector standard in the ultraviolet, vacuum-ultraviolet, and soft-x-ray spectral ranges," Appl. Opt. **36,** 5421–5440 (1997).
22. P. S. Shaw, K. R. Lykke, R. Gupta, T. R. O'Brian, U. Arp, H. H. White, T. B. Lucatorto, J. L. Dehmer, and A. C. Parr, "New UV radiometry beamline at the Synchrotron Ultraviolet Radiation Facility at NIST," Metrologia **35** (1998).
23. J. Geist, E. F. Zalewski, and A. R. Schaefer, "Spectral response self-calibration and interpolation of silicon photodiodes," Appl. Opt. **19,** 3795–3799 (1980).
24. J. Geist, D. Chandler-Horowitz, A. M. Robinson, and C. R. James, "Numerical modeling of silicon photodiodes for high accuracy applications, Parts I, II, and III," J. Res. Natl. Inst. Stand. Technol. **96,** 463–492 (1992).
25. D. L. Ederer, B. E. Cole, and J. B. West, "A high-throughput 2-m normal incidence monochromator for SURF II," Nucl. Instrum. Methods **172,** 185–190 (1980).
26. L. R. Hughey, "Improved resolution and flexibility of the SURF II high-throughput 2-m normal incidence monochromator," Nucl. Instrum. Methods A **347,** 294–298 (1994).
27. L. P. Boivin and K. Gibb, "Monochromator-based cryogenic radiometry at the NRC," Metrologia **32,** 565–570 (1995/1996).
28. Certain commercial equipment, instruments, or materials are identified in this paper to foster understanding. Such identification does not imply recommendation or endorsement by the National Institute of Standards and Technology nor does it imply that the materials or equipment identified are necessarily the best available for the purpose.
29. B. N. Taylor and C. E. Kuyatt, "Guidelines for evaluating and expressing the uncertainty of NIST measurement results," NIST Tech. Note 1297, 2nd ed. (National Institute of Standards and Technology, Gaithersburg, Md., 1994).
30. T. Saito, K. Katori, M. Nishi, and H. Onuki, "Spectral quantum efficiencies of semiconductor photodiodes in the far ultraviolet region," Rev. Sci. Instrum. **60,** 2303–2306 (1989).
31. R. Korde and J. Geist, "Quantum efficiency stability of silicon photodiodes," Appl. Opt. **26,** 5284–5290 (1987).
32. L. Fu and J. Fischer, "Characterization of photodiodes in the UV and visible spectral region based on cryogenic radiometry," Metrologia **30,** 297–303 (1993).
33. C. L. Cromer, T. B. Lucatorto, T. R. O'Brian, and M. Walhout, "Improved dose metrology in optical lithography," Solid State Technol. **39,** 75 (1996).
34. K. Solt, H. Melchior, U. Kroth, P. Kuschnerus, V. Persch, H. Rabus, M. Richter, and G. Ulm, "PtSi-n-Si Schottky-barrier photodetectors with stable spectral responsivity in the 120 nm to 250 nm spectral range," Appl. Phys. Lett. **69,** 3662–3664 (1996).
35. T. R. O'Brian, "SURF III: the next generation radiometric storage ring facility at NIST," in *Ultraviolet Atmospheric and Space Remote Sensing: Methods and Instrumentation*, R. E. Huffman and C. G. Stergis, eds., Proc. SPIE **2831,** 222–228 (1996).